



HAL
open science

Experimental analysis of multiphase flow in metallic foam: flow laws, heat transfer and convective boiling

Frederic Topin, Jean-Philippe Bonnet, Brahim Madani, Lounes Tadrist

► To cite this version:

Frederic Topin, Jean-Philippe Bonnet, Brahim Madani, Lounes Tadrist. Experimental analysis of multiphase flow in metallic foam: flow laws, heat transfer and convective boiling. *Advanced Engineering Materials*, 2006, *Metal Foams*, 8 (9), pp.890-899. 10.1002/adem.200600102 . hal-00343852

HAL Id: hal-00343852

<https://hal.science/hal-00343852>

Submitted on 1 Feb 2022

HAL is a multi-disciplinary open access archive for the deposit and dissemination of scientific research documents, whether they are published or not. The documents may come from teaching and research institutions in France or abroad, or from public or private research centers.

L'archive ouverte pluridisciplinaire **HAL**, est destinée au dépôt et à la diffusion de documents scientifiques de niveau recherche, publiés ou non, émanant des établissements d'enseignement et de recherche français ou étrangers, des laboratoires publics ou privés.

Experimental analysis of multiphase flow in metallic foam: flow laws, heat transfer and convective boiling.

Frédéric Topin, Jean-Phillipe Bonnet, Brahim Madani, Lounès Tadrist

Ecole Polytechnique Universitaire de Marseille - Laboratoire I.U.S.T.I - CNRS- UMR 6595 Université de Provence - Technopôle de Château-Gombert - 5, Rue Enrico Fermi 13453 Marseille Cedex 13 – France

The first part of this work deals with flows laws of gas, liquid and mixture in metallic foam. This experimental work is based on the stationary pressure profile measurement in a channel filled with metallic foam of several grade or material for several controlled flow rates. Several foam samples with different characteristics (10, 40, 60, 100 PPI) of copper or nickel are studied. In single-phase conditions, we evaluate permeability and inertial coefficient according to the Forchheimer model. In the gas flow case, compressibility effects are taken in account. Emphasis is given on the relative contributions of inertial and viscous effect. The specific behavior linked to compressibility effect is thoroughly studied. The adiabatic (air-water) conditions are analyzed; the results are reported in term of biphasic multipliers according to a simple homogeneous model to study the impact of foam texture and gas quality on flow laws. Several aspects of the two-phase flow case (i.e. liquid-vapor) are discussed: phase repartition, pressure drops, characteristic boiling curve.... In monophasic conditions, the heat transfer coefficient was improved by two orders of magnitude by the presence of metallic foam with only a limited increase of pressure drop. In biphasic condition, the study of convective boiling regime also showed significant heat transfer enhancement with very low-pressure drop. A simple one dimensional homogeneous model was used and allows a good description of global flow behavior across the test section.

Keywords: *metallic foam, flow laws, transport properties, convective boiling*

1. Introduction

Metal foams are a relatively new class of materials with low densities and attractive thermal, mechanical, electrical and acoustic properties [1]. They are widely quoted to present a random topology, high open porosity, low relative density and high thermal conductivity of the cell edges, large accessible surface area per unit volume. All these characteristics make metal foam heat exchangers efficient, compact and light weight. Moreover, they also promote mixing and have excellent mechanical properties. Metallic foams uses and applications have been widening quickly during the last few years and they are proposed for use in numerous applications such as compact heat exchangers, reformers, biphasic cooling systems and spreaders for increasing heat transfer; improve mixture and chemical reaction [2-4]. Different types of metal foams are used as a buffer between a stiff structure and a

fluctuating temperature field. They are also used in geothermal operations and in petroleum reservoirs [5]. Ceramic foams are used in advanced burners and heat pipes. Foams have been used in high-power batteries for lightweight cordless electronics, and catalytic field application such as fuel cells systems [6]. Due to their novelty, peculiar structure and varied manufacturing processes, metal foams are still incompletely characterized. Accurate evaluation of these properties becomes critical for various uses.

The control of the texture of porous materials used for the optimization of given application represents a significant technological stake. Accurate determination of transport properties (in respect with convenient geometrical parameters) is needed for both single phase and boiling conditions flows in order to understand transport phenomena in these materials and eventually optimize their texture for given application. Models widely used for low porosity media are more difficult to apply to high porosity materials.

Most of the works dealing with foam transport properties are based on arbitrary periodic structures which represent with variable degree the real texture of the foam. The morphology of such open-celled structure is often characterized using cell ligament diameter or pore size and the relative density. [7, 8] assumed a rectangular distribution of solid material in a representative unit cell. Several authors [9-11] used a simple cubic cell consisting of slender cylinder as edges. Dimensions of the representative unit cell are obtained in function of relative foam density. Analogy between flow through the foam and through a bank of cylinders is used to derive analytical expressions for pressure drop [12]. More complex periodic structure were tested using 3D numerical simulation of flow through idealized open-celled metal foam [13]. Thus, model remains, yet only qualitative [14-19].

During the last decade, numerous experimental and theoretical works on single-phase flow in cellular material have been lead. It exists, on the other hand far less data about hydrodynamics of gas/liquid flow in such media. Moreover it appears a strong dispersion of literature results which limit the development and validation of model of flow properties in function of geometrical parameters of such foam(see, e.g. review given by [20]). Data of the literature reported that metal foams of grade and porosity exhibit extremely different transport properties. Friction coefficient variations versus Reynolds

number (both based on pore size: ($\lambda = \frac{2\Delta P d_p}{L\rho U^2}$ and $Re = \frac{U d_p}{\nu}$) as reported by [20] are plotted on figure

1. The divergence of these coefficients measured for metallic foam samples of comparable porosities and grade (PPI) is obvious on this figure. The values of friction factor differ from more than 1 decade depending on Reynolds number. These discrepancies in experimental results and theoretical models, can be attributed to the lack of in one hand, to the experimental procedures used to determine the hydrodynamic properties of these materials and in the other hand, to the lack in methods allowing accurate determination of metallic foam microstructure characteristics related to flow/transport properties.

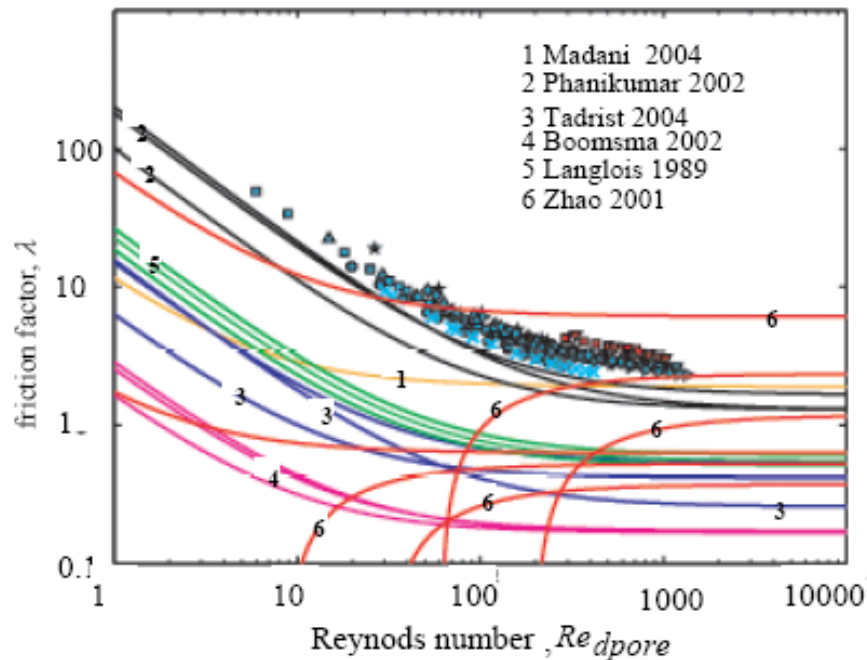


Figure. 1 Friction factor versus Reynolds Number (both based on Pore diameter).

Lines: literature data[13, 20-23], Symbol: present work all samples, air and water results.

We present here, experimental studies aiming at estimate characteristic transport properties of metallic foam in order to correlate them to their morphology [24, 25]. The flow properties are analyzed for these foams: permeability, inertial coefficient, friction factors. Several aspects of adiabatic two-phase flow are discussed. The second part is devoted to single-phase heat transfer and characterization of convective boiling phenomena (i.e. liquid-vapor).

2. Single-phase Flow

2.1. Experimental Set-Up

This experimental work is based on the stationary pressure profile measurement in a channel filled with metallic foam of various grade or material and crossed by controlled flow rates. Several foam samples with different characteristics (grade from 10 up to 100 PPI) of copper, nickel, or allied nickel are studied (see Table 1 for details). This experimental set-up is designed, to study the impact of the solid matrix on flow phenomena in the foam in both single-phase and adiabatic two-phase flow conditions. This apparatus consists of three main parts: test section, fluid loop and data acquisition system as shown on figure 2.

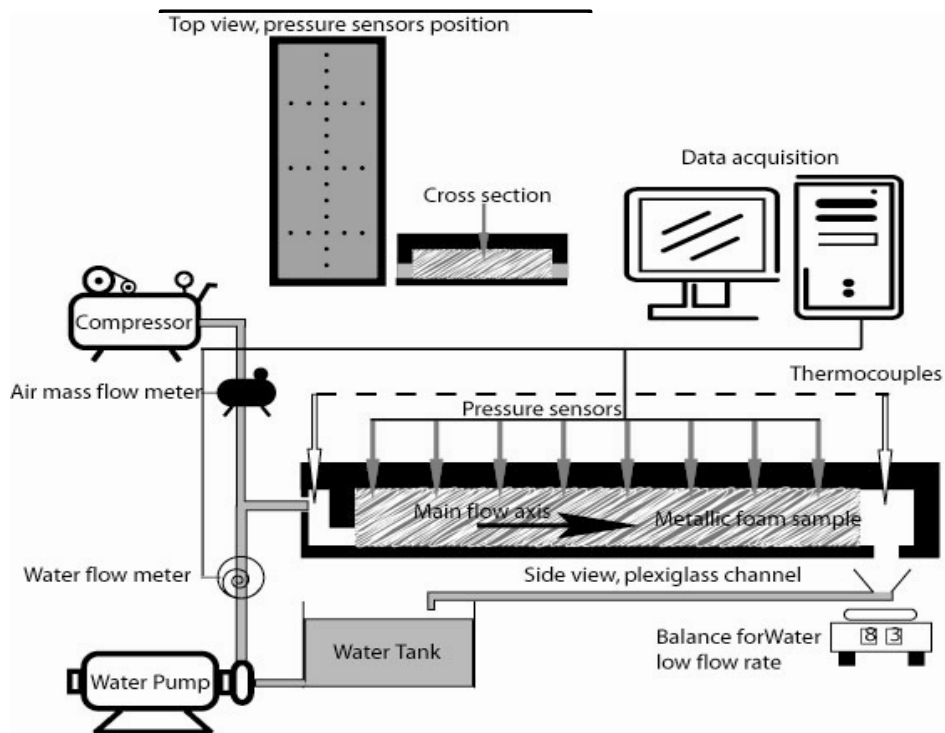


Fig. 2 Experimental set-up for single-phase and adiabatic two-phase flow laws characterization.

The test section (250 mm length, 50 mm wide and adjustable height) is instrumented with 12 pressure sensor (Sensym®, sensitivity $2.6 \mu\text{V}$ per Pa) placed every centimeter along the main flow axis. Additional pressure sensor are placed along 3 lines perpendicular to the flow direction to assess the one-dimensional nature of the flow. Foam samples (whose lengths vary from 130 up to 200 mm) are placed

in the central part of the channel in order to keep a tranquilization zone upstream and downstream of the sample. Test section is placed horizontally in order to avoid uncertainties due to hydrostatic effects [20]. The liquid fluid loop is constituted by a storage tank (50 l capacity) and a variable velocity gear pump which can give a constant flow rate in the range of $0-10^{-4} \text{ m}^3 \text{ s}^{-1}$ independently of pump downstream conditions. Constant air flow (range $0-4 \cdot 10^{-3} \text{ Nm}^3 \text{ s}^{-1}$) is obtained using a compressor and a pressure regulation valve. The test section is connected, downstream, to a separator which is installed for the two-phase flow experiments. The liquid flows by gravity down the storage tank while the air is simply released to atmosphere. A weighted tank could be inserted in the liquid loop to assess the mass flow rate. Liquid flow rate is monitored (upstream of the test section) using two turbine flow meters (Mac-Millan®) for optimal accuracy over the full range of experiments. The first one works in the range of $3.33 \cdot 10^{-5} - 8 \cdot 10^{-5} \text{ m}^3 \text{ s}^{-1}$ and the other one in the range $1.6 \cdot 10^{-6} - 3.33 \cdot 10^{-5} \text{ m}^3 \text{ s}^{-1}$. The weighting device arranged in downstream of the test section has a sensitivity of about 1 g and a capacity of 3 l. Air flow is monitored upstream of the test section using three mass- flow meters (Aalborg®) respective operating range : 0-50, 0-100 and 0-250 Nl/min. An accuracy of about 0.1 % overall flow rate range is thus obtained. Hydrodynamic (null flow) profile is checked before and after each experiment in order to eliminate all offset between pressure sensors. Pressures, temperature and inlet flow rate of both fluid (air and water) are continuously monitored.

The same experimental procedure is used for all tests. Before each series of measurement, the foam sample was flooded a long times ensuring initial wetting (water) or drying (air), and established flow. The fluid is then, maintained on circulation for about half an hour after system has reached a stationary regime. Hydrodynamic (null flow) profile is checked before experiment in order to eliminate all offset between pressure sensors. For each measurement, an averaging procedure (averaging time 1minute, data acquisition 500 Hz) is used to reduce measurement noise, after checking stationary behavior of pressure and flow rate signal. Accuracy of pressure measurement is better than 5 Pa [20].

After each measurement series, the flow is stopped and the hydrostatic pressure profile is measured anew and compared to the previous hydrostatic one. In this way we could ensure that pressure sensors

bias has not changed with the time.

Gravity and capillarity driven flow through cell edges during the manufacture of metallic foams induce material property gradients (tortuosity, cell size...) and cells themselves are not spherical [26]. Slight anisotropy of geometrical parameters is observed for our sample. Nevertheless at this stage of the study we neglect these effects. Measurement of full permeability and inertial coefficient tensor is, yet, difficult and the precision of our set-up in the studied configuration doesn't allow measurement of transverse pressure gradient with an accuracy compatible with the objectives of this work [27].

2.2. Flow law

It is well established that flows at very low flow rates through a porous medium are governed by Darcy's law [28]. For homogeneous porous media, "high-velocity" flows are characterized by a nonlinear relationship between the pressure drop and the flow rate. At high Reynolds number the empirical Forchheimer equation is used to account for the deviation from Darcy's law [29]:

$$-\frac{dP}{dz} = \frac{\mu}{K}u + \beta \rho u^2 \quad (1)$$

Where ρ is the fluid density, K (permeability; m^2) and β (inertial coefficient; m^{-1}) are intrinsic parameter of the solid matrix and depend only on its structural properties. In this formulation the Brinkman correction is neglected. That means that the pressure drop is considered as the sum of two terms: viscous (u , Darcy law) and inertia (u^2) terms. The pressure gradient across the foam is a function of system geometry (porosity, pore and ligament size...), and physical properties of the fluid phase (viscosity, density). We measured the pressure drop using two different fluids: a liquid (water) and a gas (air) in order to confirm that, K , β are independent of the fluid nature (Table 1).

2.3. Pressure profiles-Compressibility effects

As we measured pressure profiles along the main flow axis, we could check sample heterogeneities, entrance effects and non-linearity due to compressibility effects [20, 30]. In the water flow case, for all tested samples, a linear regression fit with a very good accuracy the experimental pressure profiles. Residual of these interpolations are always negligible and comparable to measurement noise. On the

other hand, in gas flow case, experimental data shown that pressure drop versus position is clearly not linear. As air flow compressibility effects are not negligible because $\Delta P/P \approx 1$ [31] pressure profiles gradient vary along main flow axis (Figure. 3). The curvature of pressure profile increases with pressure difference; this effect is thus maximal for the smallest pore size samples.

Sample	Pore diameter d_p [μm]	Porosity ϵ	Specific surface Sp [m^2/m^3]	Water permeability K_{Water} [m^2]	Air permeability K_{air} [m^2]	Permeability K_{WA} [m^2]	Water inertia coefficient β_{Water} [m^{-1}]	Air inertia coefficient β_{air} [m^{-1}]	Inertia coefficient β_{WA} [m^{-1}]
Ni 100	500			1.63E-09	1.42E-09	1.38E-09	1670	2010	1686
Ni10	4429		680	2.00E-07	5.76E-08	7.63E-08	272	261	248
NC 4753	400	0.9	5600	2.28E-09	1.85E-09	2.01E-09	2194	2138	2175
NC 3743	569	0.87	5303	2.68E-09	2.13E-09	2.11E-09	1622	1330	1329
NC 2733	831	0.91	3614	6.19E-09	4.44E-09	4.79E-09	1130	1075	1088
NC 1723	1840	0.88	1658	2.32E-08	2.81E-08	1.14E-08	631	490	446
NC 1116	2452	0.89	1295	2.98E-08	6.02E-08	3.62E-08	400	381	364
Cu 40	1500	0.95		1.62E-08	1.22E-08	7.20E-08	783	1000	1107
Cu 45 (a)	1000			4.49E-09	6.09E-09	5.30E-09	1056	1281	1167
Cu 45 (b)	1000			6.20E-09	7.58E-09	3.62E-09	1139	1615	1133
Cu 45(c)	900				5.35E-09			1768	
Cu 10	4055	0.92	758		8.17E-08			201	

Table 1 : Flow laws parameters & sample properties.

Cu 45 (a) standard; Cu 45 (b) increased surface roughness, Cu 45 (c) washcoated with alumina

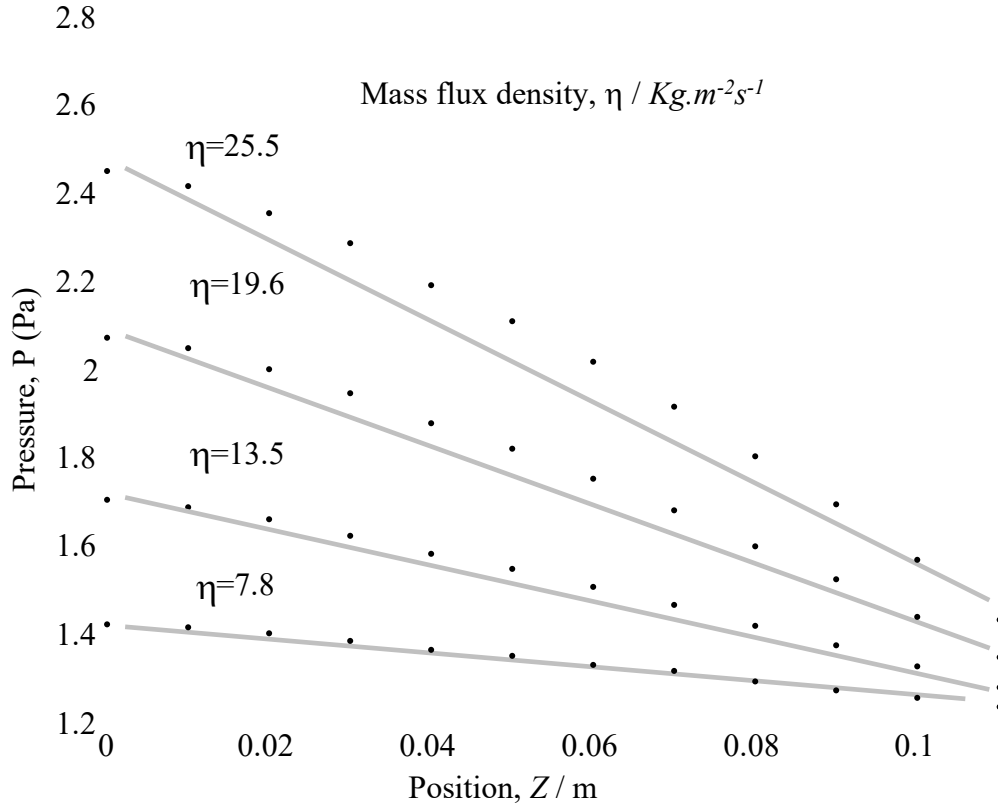


Figure 3 Pressure profiles in air flow- compressibility effect. Sample NC 4753
Grey lines: linear approximation

We identify parameters of Forchheimer equation (1) which takes the following forms using mass flux η :

$$-\frac{d\rho P}{dz} = \zeta \left(\frac{\mu}{K} \eta + \beta \eta^2 \right) \quad (2)$$

$$\zeta = 2 \text{ Perfect gas}, \zeta = 1 \text{ Liquid}$$

The “density x pressure” (called “ ρP ” in the following text) profiles along main flow axis are linear at all tested velocities and for both fluids. Thus, for a given sample, the gradient of this quantity depend only on mass velocity. Except near inlet (entrance effect, flow not established) the gas case, linear regression of “ ρP ” versus the position fit with a very good accuracy the different profiles. Thus, the gradient of this quantity depend only on mass velocity and is evaluated by linear regression on these profiles (figure 4).

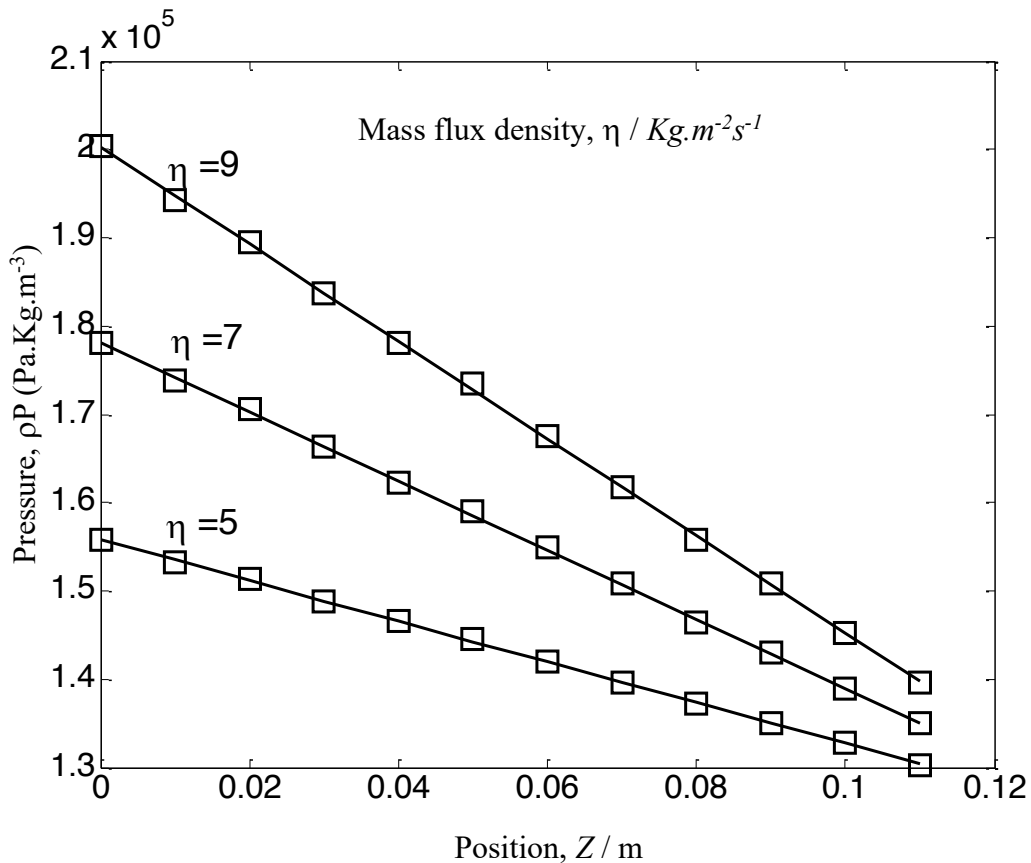


Figure 4: “ ρP ” profiles for several air mass flux densities. Sample 4753

Permeability and inertial coefficient are identified from order 2 polynomial regression of “ ρP ” gradient variations in function of mass flux. Experimental results follow, indeed, a quadratic law and deviation between experimental values and model are very low (1 up to 3 %).

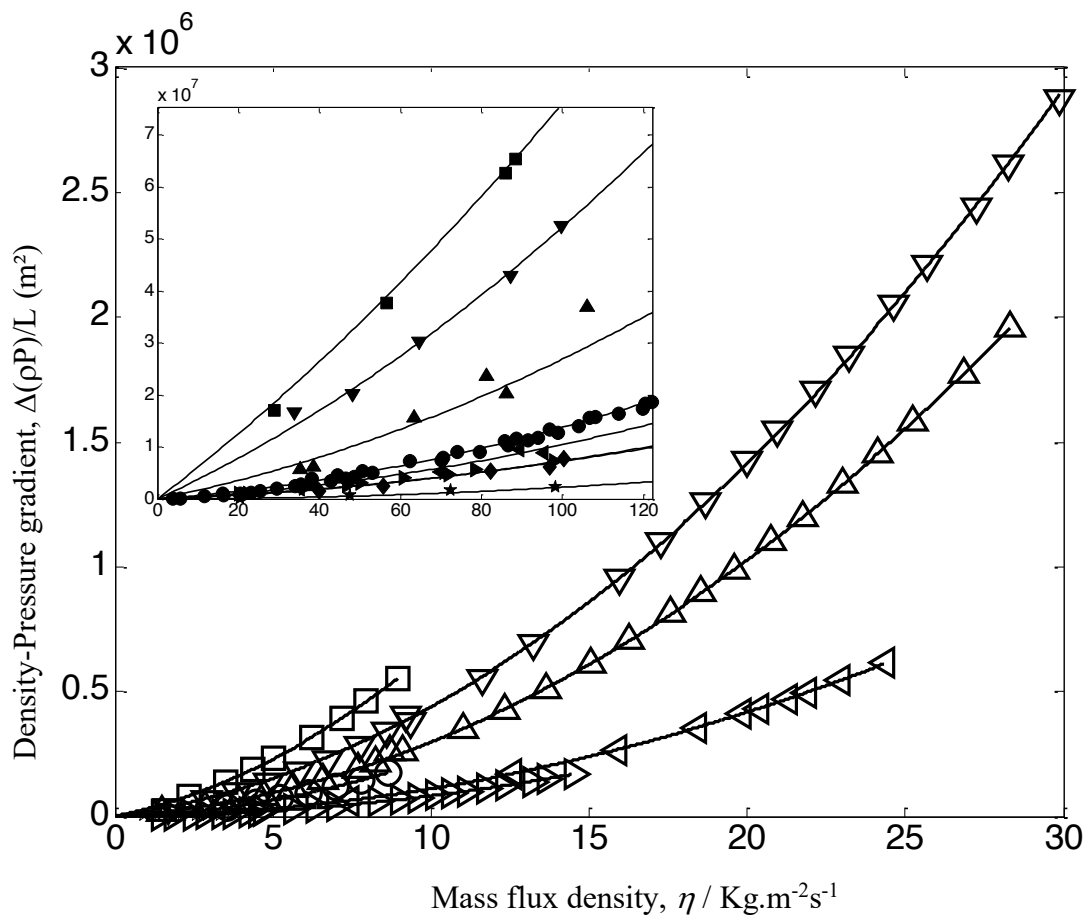


Figure 5: “ ρP ” gradient versus mass flux density (white: air; black: water).

Symbol shape correspond to sample (see fig. 7)

Figure 5 illustrate these results, on the tested range of Reynolds number (10 – 10000), experimental data are best fitted with by a quadratic law. A detailed view of region near the origin highlights the importance of inertial effects even for relatively low Reynolds number: (Re_{Dp} : 5 – 100). This holds true for each sample and indicates that in the most commonly encountered use of metallic foam Forchheimer model has to be used to model flow behavior properly. Nevertheless, using more viscous fluid, we could have acceded to very low Re_{Dp} number (<1) flow regime, and a Darcian behavior may probably have been observed. We compare the relative intensity of inertial and viscous contribution to pressure drop deduced from water flow results on figure 6. Indeed, inertial effects exist for all tested velocities. These latter even constitute the main contribution to pressure drop for the greater part of tested velocity range. This trend being accentuated for bigger pore sizes. On the other hand, even if viscous contributions are

lower than inertial one, they are not negligible in these experiments and the preponderance of viscous over inertial effects at low velocity is clearly visible, relative importance of viscous effect is inversely proportional to the pore size of these foams. Nevertheless, this ratio remains in the range (0.05 – 10) for all tested cases.

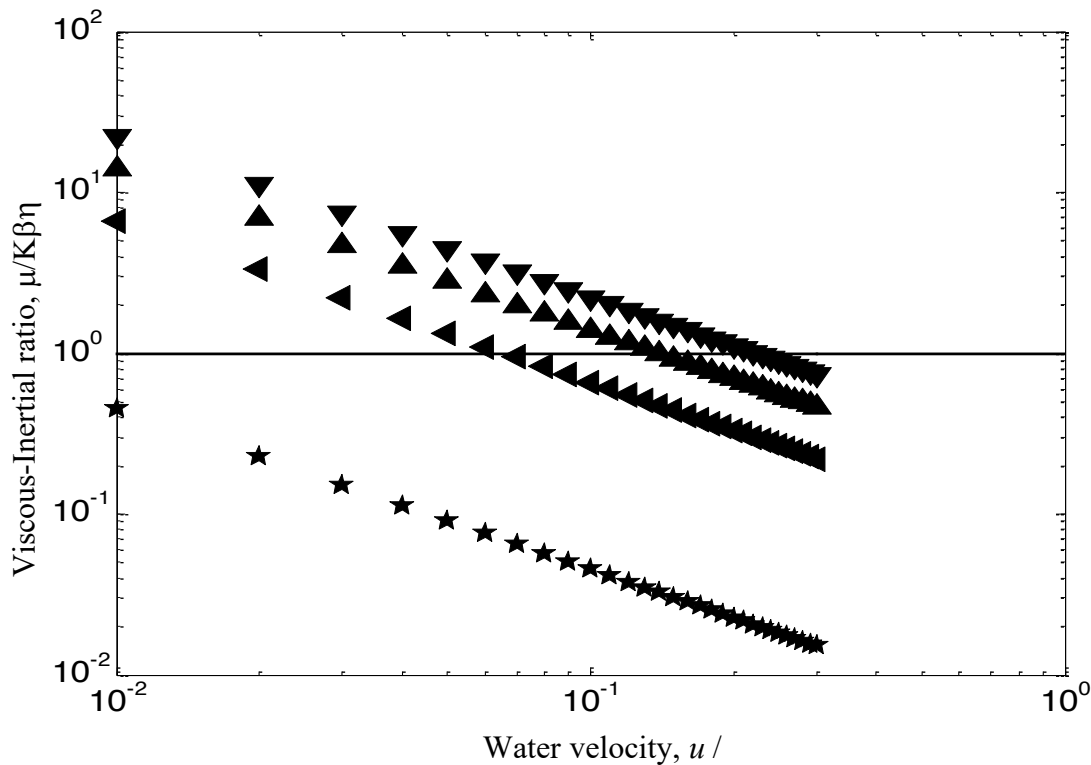


Figure 6: Comparison of relative viscous and inertia effects contribution on pressure gradient plotted versus water flow velocity for several sample (Fig. 7).

Comparing values of permeability and inertial coefficient determined using liquid (resp. gas) data alone versus values obtained using data for both fluids simultaneously show up a good agreement (Table 1). As compressibility effects have been taken into account, the nature of the fluid doesn't change the measured values even if slight differences could be observed. Although Reynolds number (based on pore size) range is identical for the two fluids the mass fluxes are quite different ($0-30 \text{ kg.m}^{-2}.\text{s}^{-1}$ for the gas and $0 - 500 \text{ kg.m}^{-2}.\text{s}^{-1}$ for the liquid) and thus may explain the difference in inertial coefficient and permeability values. Indeed the reduced pressure gradient, plotted in function of Reynolds number for all samples on figure 7, highlight that there is no influence of fluid nature on the flow laws. Similar trend are observed for all curves, that are, indeed, representative of weak inertia flow [29].

For each sample, pressure gradient asymptotically converge toward a fully inertial behavior (slope 2 on this log-log plot) at high Reynolds number. At low Reynolds, results slope decrease slightly and are expected to converge to Darcian flow (slope 1) for Reynolds inferior to one. Clearly, data obtained for the sample of greater pore size are more representative of inertial regime, thus sensibility to inertial coefficient is better in this case. On the other hand, for the smaller pore size this flow is more representative of a viscous one (even if inertial effects exist). This indicates that K and β estimation is not always done in an optimal way. Uncertainties on K and β are consequently different depending on pore size. Nevertheless, most of the data are, indeed representative of transition zone.

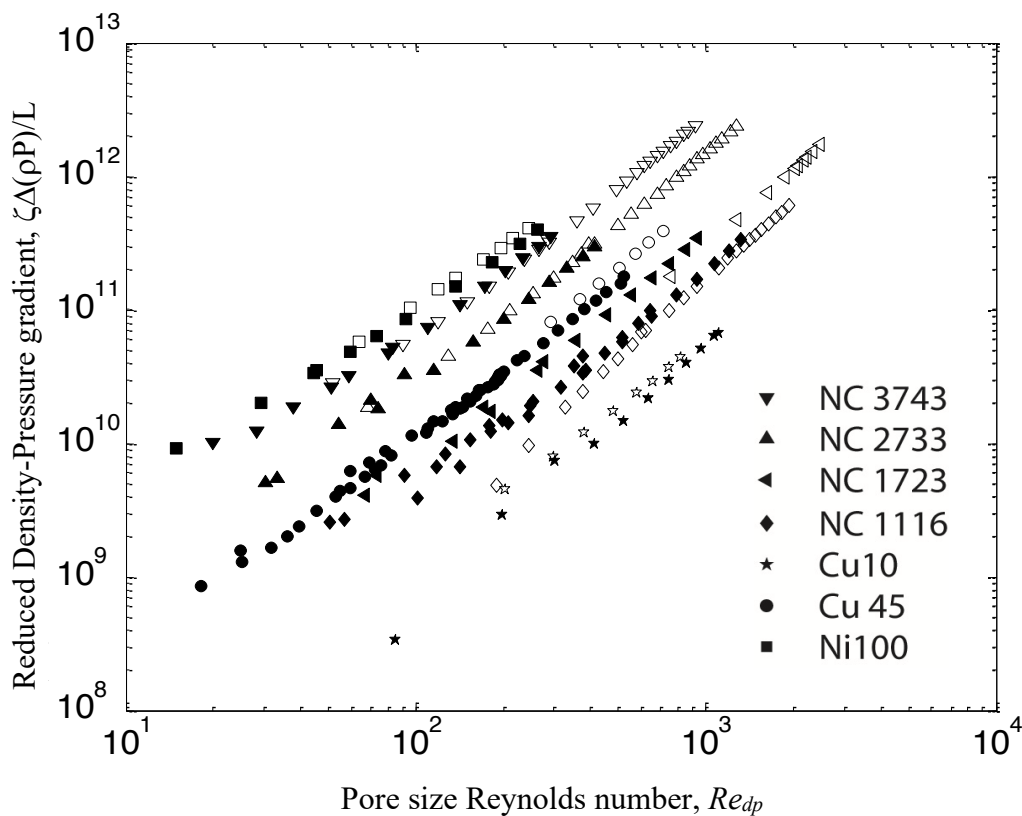


Figure 7: Reduced pressure drop versus Reynolds number (pore size) – air (white) and water (black) flow data. Shape of symbol indicates sample

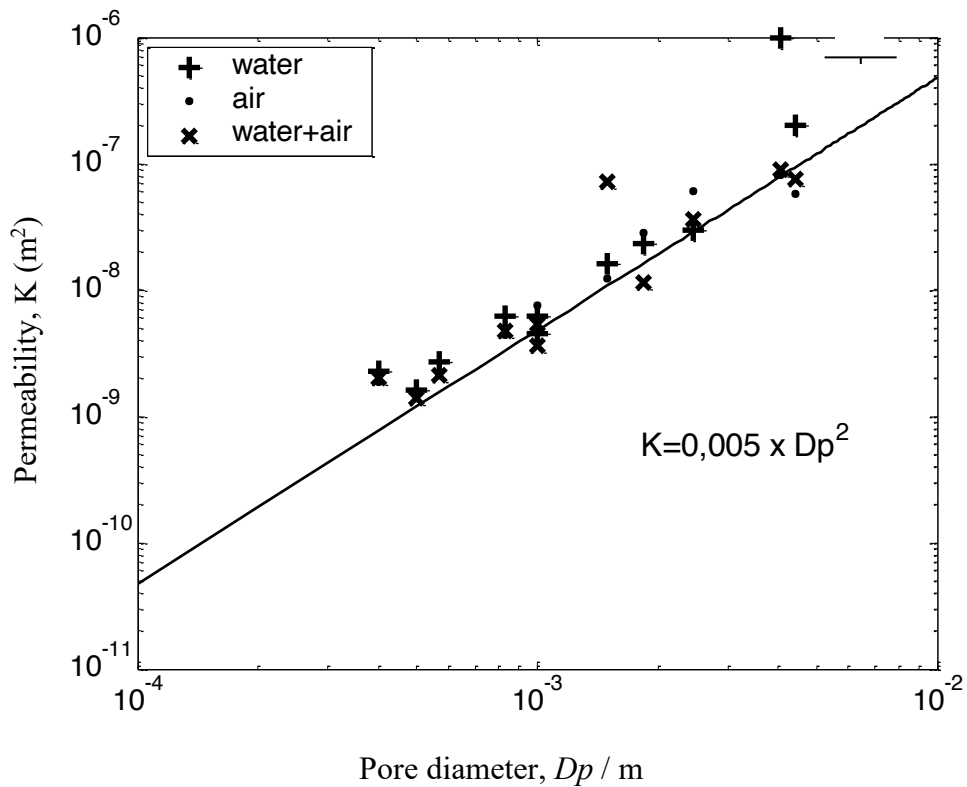
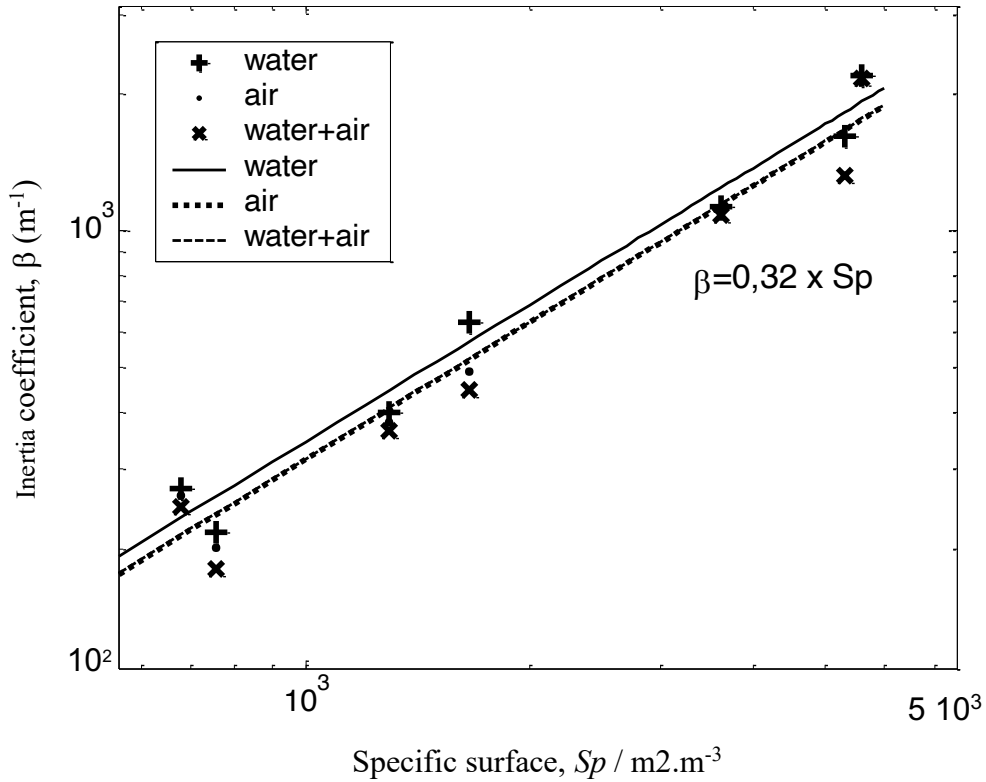


Figure 8: Variation of inertia coefficient versus specific surface (up).
 Variation of permeability versus pore diameter (down).

2.4. Flow law parameters

K and β coefficients depend on porosity, pore diameter strut size, specific surface... Analysis of our

experimental data allows us to determine the main parameter governing the variations of permeability and inertial coefficient. Viscous effects are governed by pore size while it is the specific surface that produces the best fit of our results with an Ergun like law [3].

$$K = \zeta \frac{\varepsilon^3 d^2}{(1-\varepsilon)^2} \text{ and } \beta = \xi S_p \text{ with } \zeta = 1.391 \cdot 10^{-4} \text{ and } \xi = 1.32 \quad (3)$$

Inertial pressure drop are linked to acceleration (direction and magnitude). Indeed microscopic flow in foam could be modeled by flow around obstacle. Thus the natural parameters to describe such flow are strut diameter and pores size thus specific surface. Figure 8 show the experimental results and the model. A good agreement is observed.

2.5. Comparison with literature data

We compare our results to literature data [3, 10, 13, 15, 22, 23, 32-36] gathered [20]. As shown in figure 1, the major part of works gives similar trend of pressure drop coefficient but results obtained for similar foam are scattered on a rather wide range. Some data are obtained using liquid flow [32] and several authors gives results obtained with gas flow. [3, 10, 14, 15, 23]. The commonly used technique to determine flow law in porous media is to evaluate pressure gradient using only inlet and outlet pressure Moreover several results obtained with gas flow neglect compressibility effect even when $\Delta P/P$ is not nil, at high velocity regimes. This leads to an important dispersion of results and even to aberrant (non-physical) values of the permeability.

Analysis of permeability data in function of porosity for several pore densities highlights the wide dispersions of permeability as expected from error analysis [20]. Nevertheless, some trends could be inferred: permeability decreases slightly as the pore density increases and increases slightly as the porosity increases. Anyway, these variations should be considered with caution as uncertainties are greater than the observed variations.

Figure 9 shows inertial coefficient versus pore size for several ligaments diameters. On this figure, we can notice that β decreases as pores and ligament diameters increase. Upon data gathered from the

literature,. The inertial coefficient is given proportional to the pore density and inversely proportional to the ligaments and pore diameters. In opposite, using the gathered data base, we can not detect any clear relation linking inertial coefficient to the porosity. These observations derived from the literature results need to be analyzed systematically. They must be carried out using well known geometrical characteristics of metallic foams

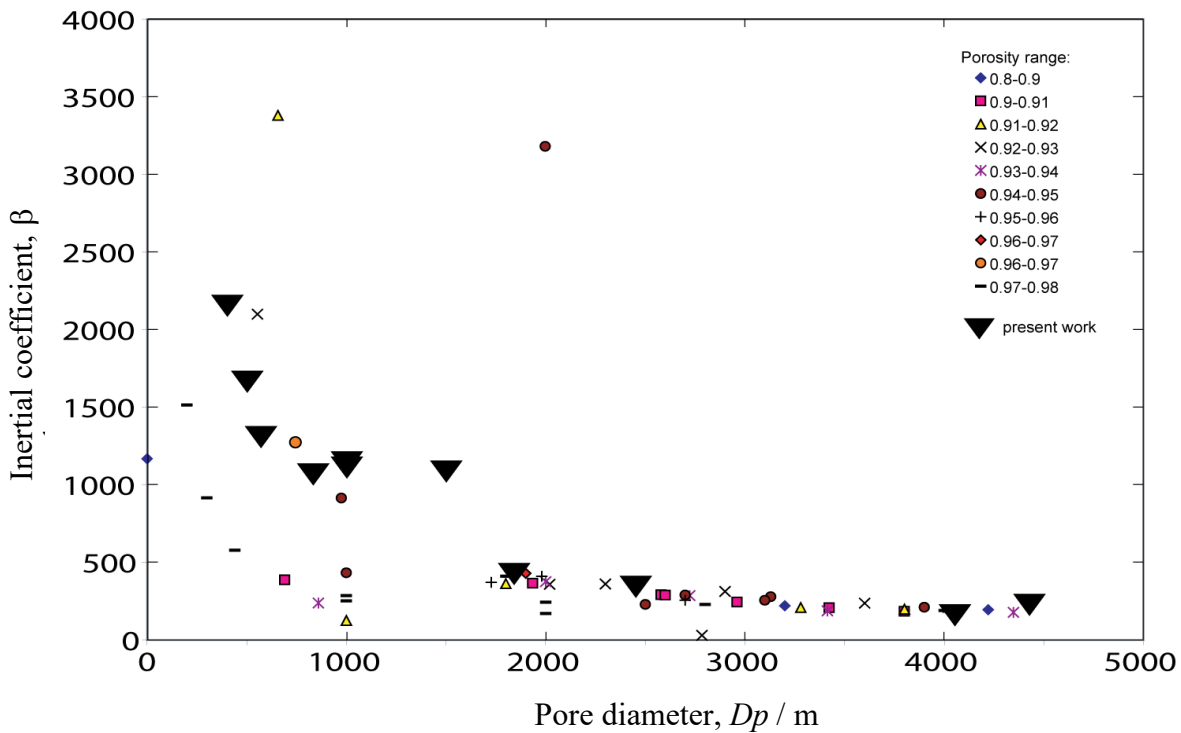


Figure 9: Variation of inertia coefficient versus pore diameter. Comparison with literature.

3. Adiabatic Two-phase Flow

3.1. Pressure Drop

We present on figure 10 the results concerning pressure losses obtained for air-water mixture flow in foams. The gas quality of the flow is our experiments vary from 0.5 up to 25 % and the void fraction (evaluated from a no-slip model) is in the range 80 up to 99%. The compressibility effects should thus appear clearly on two-phase pressure profile as the mixture is mainly composed of gas. Due to density variation with local pressure the mixture velocity should increase from inlet to outlet producing an increasing pressure gradient. But, as experimental results are correctly modeled by linear

approximation, it should exist an antagonist effect (void fraction variation probably) that mask this behavior.

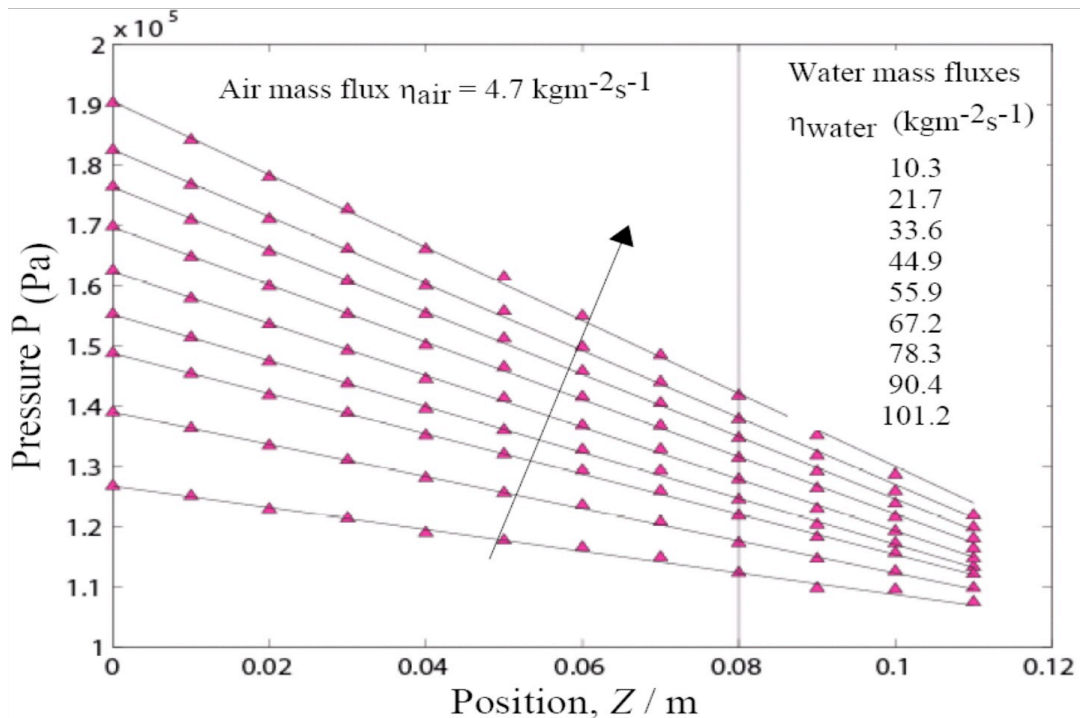


Figure 10: Two-phases flow pressure profile. Sample Ni100

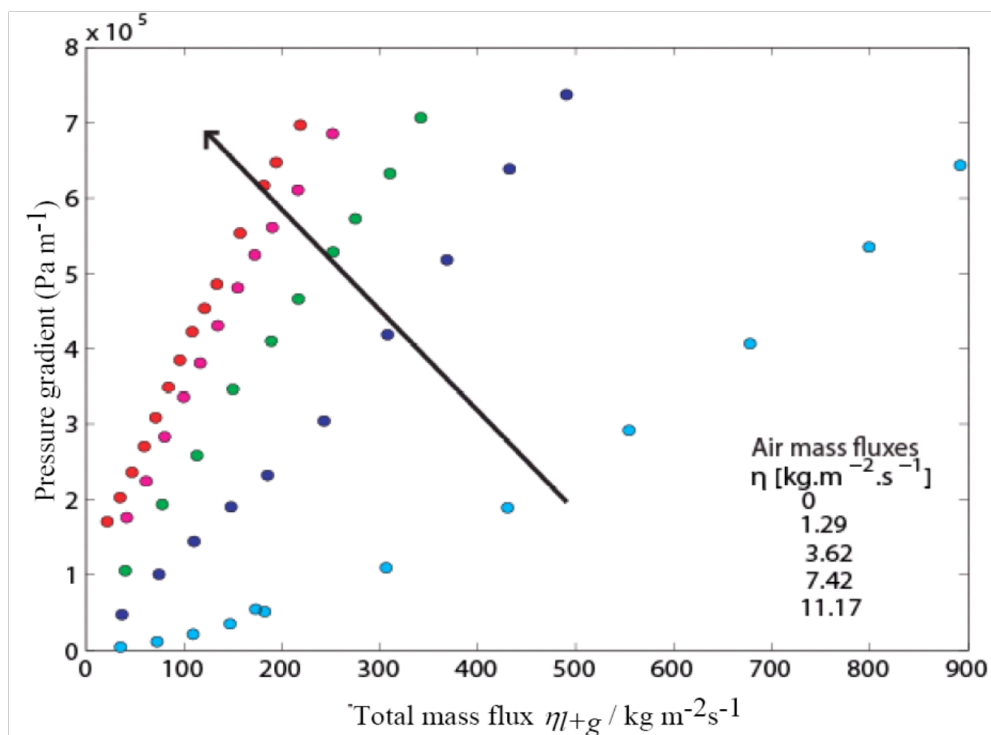


Figure 11: Biphasic pressure gradient versus total mass flux variations for several air mass fluxes

Figure 11 illustrates the influence of air flow rate on biphasic pressure gradient. For a given total mass

flux the pressure loss is proportional to air flow rate. In other words, pressure gradient is proportional to flow quality. The curvature of these curves is inversely proportional to the quality of the flow. This indicates that viscous effects depend more strongly on quality than inertial one.

3.2. Biphase Multiplier

We do not find any other data in literature for biphase flow in metallic foam and it do not exist, yet, agreement on a model of biphase flow in porous media [12, 37-39]. Thus in order to compare our results to reference cases we choose, considering the very high porosity of the foam to compare to two-phase flow in tube. The flow is established in the studied zone and is globally one-dimensional. Taking into account the precise structure of the two-phase flow is not yet possible as both slip velocity and void fraction could not be measured. Consequently we suppose that the mixture behave as an incompressible homogeneous fluid with null slip velocity. The pressure losses of the mixture are thus described using the biphase multiplier approach [31], with x flow quality (gas mass flux/total mass flux) :

$$\phi_{LS}^2 = \frac{-(dP/dz)_{L+G}}{-(dP/dz)_L} = (1+x \left(\frac{\rho_l}{\rho_g} - 1\right)) (1+x \left(\frac{\mu_l}{\mu_g} - 1\right))^{-\gamma} \quad (4)$$

Using the experimental values of biphase multiplier are simply calculated by forming the ratio of biphase pressure drop over single-phase one. An adjustment of exponent ($\gamma \sim -0.7$) of the viscosity term appearing in the biphase multiplier expression allows to model all experimental data with reasonable agreement. Figure 12 present the comparison of experimental results with the correlation proposed by Mac Adams ($\gamma = -0.25$) for laminar flow in tubes [31]. All experimental data are roughly located on a unique curve similar to the literature correlation. Nevertheless a slight influence of pore size is visible on this figure. When pore size increase the biphase multiplier seems to be closer to the value obtained for tube. But more experimental data are needed to interpret this effect. This approach has been applied with reasonable agreement in convective boiling case, using biphase multiplier given by Mac Adam correlation [40].

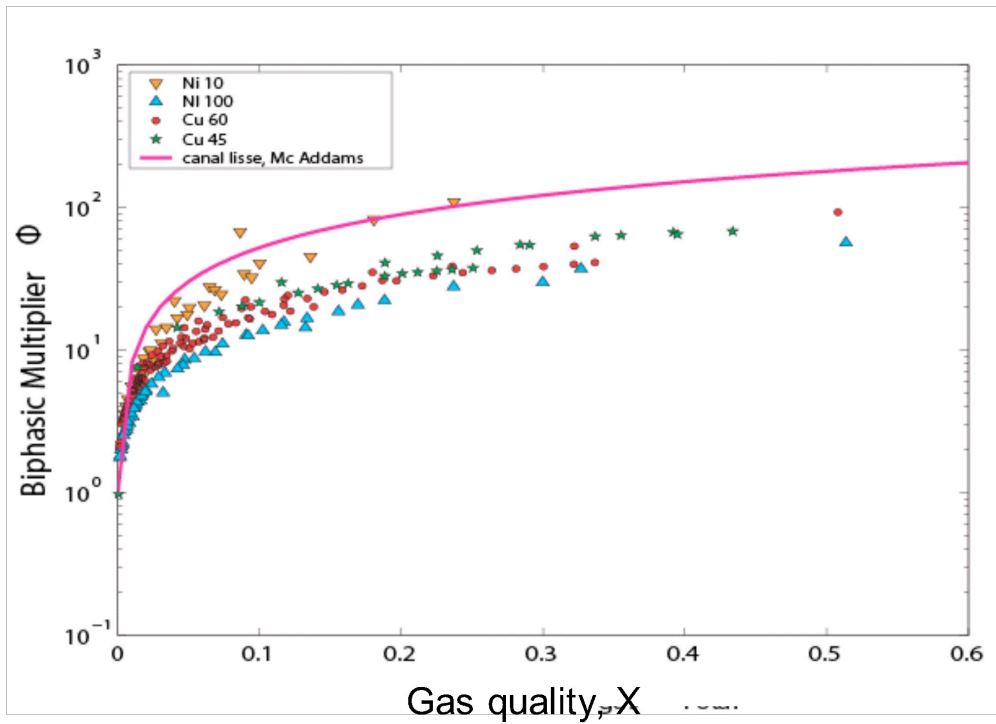


Figure 12: Biphasic multiplier versus quality. Comparison with tube correlation

Figure 13 presents a comparison of calculated and measured pressure profile obtained for one flow rate and two different heating power in case of convective boiling of n-pentane.

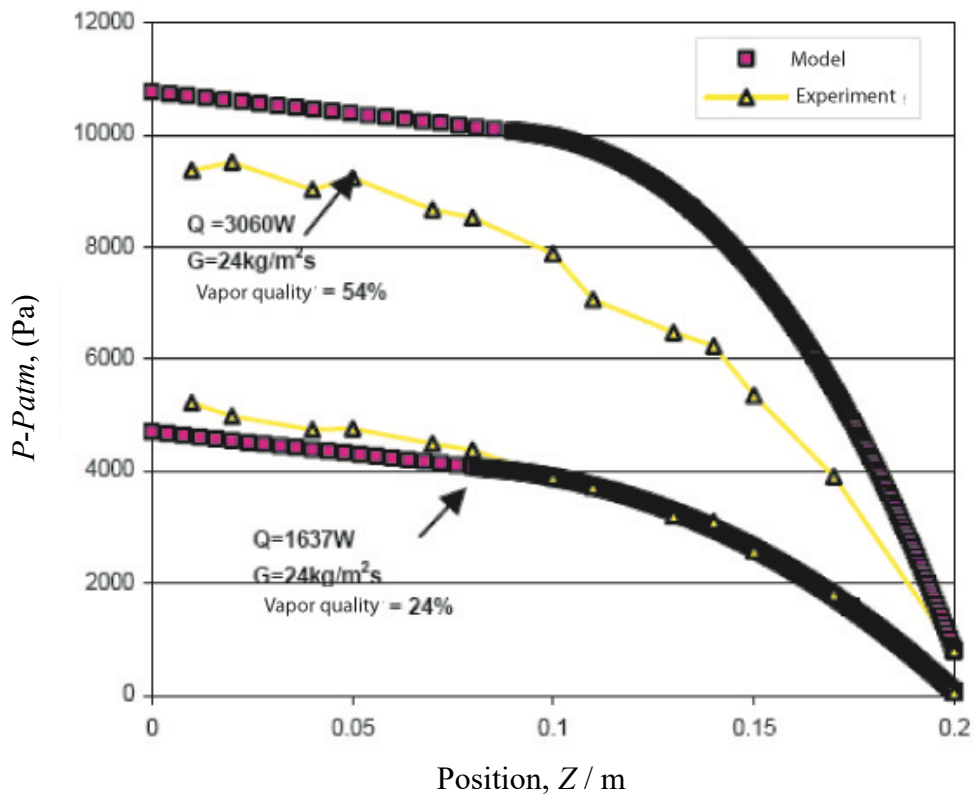


Figure 13 Measured an calculated pressure profile in convective boiling experiments [40]

The model predict with a good accuracy the pressure profile at moderate heating power.. On the other hand a clear discrepancy between experiment and model is observed at higher heat flux. This is probably due to flow regime transition at high vapor quality. Globally, the model predict with reasonable accuracy (20 % error max) the global pressure drop of the channel but is not usable to determine local pressure profiles

4. Convective Boiling

4.1.Experimental Set-Up

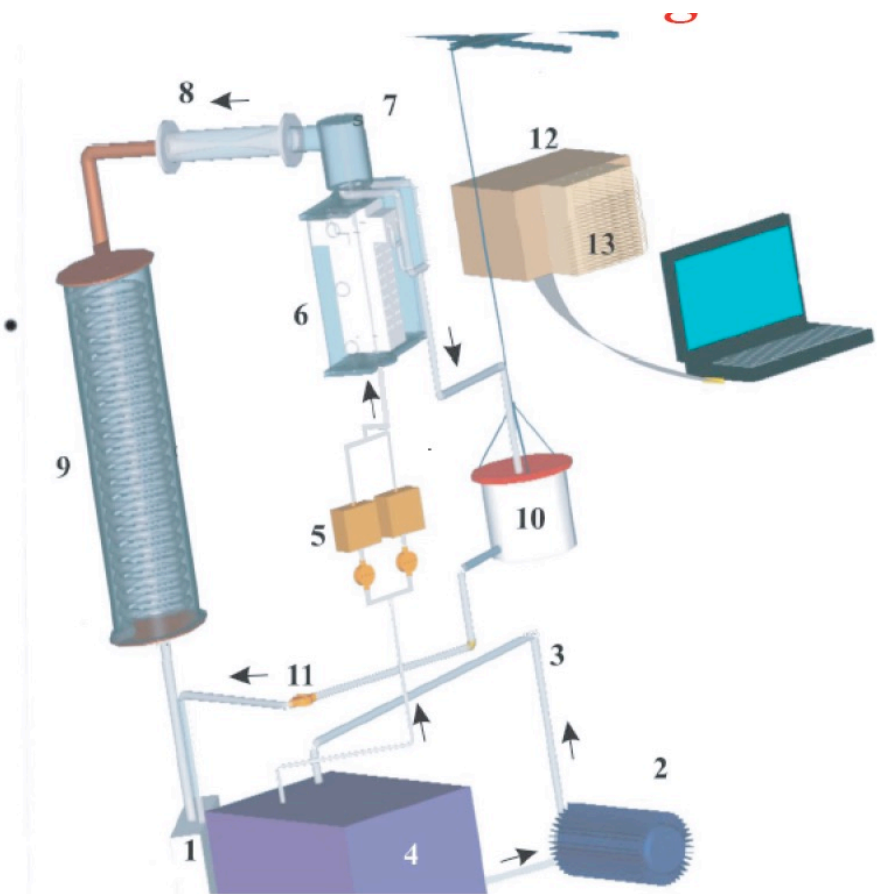


Figure 14: Experimental set-up for boiling experiments [40].

1. Storage tank, 2. Gears pump, 3. Tube, 4. Cryostat, 5. Flowmeters, 6. Test section, 7. Cyclone, 8. Venturi, 9. Condenser, 10. Weighted tank, 11. Valve, 12. Data acquisition, 13. Pressure sensors. Not shown thermocouples

The boiling mechanisms in copper foam and the evaluation of the impact of the solid matrix on flow and heat transfer phenomena were experimentally studied. It consisted of 2 rectangular channel

(10x50x100 (resp.200) mm) that contained a 40 PPI grade copper foam. The smallest one is welded to the wall, as the other is just inserted in the channel A liquid (i.e., n-pentane, low toxicity, low boiling point: 36 °C at atmospheric pressure, low phase-change enthalpy) flowed through the porous media vertically from the bottom to the top (figure 14). The channel was instrumented with 40 thermocouples and 15 pressure sensors [40, 41]. Before each experiment, we apply repeated Boiling-cooling sequence in order to eliminate non-condensable substances, then flow is imposed at the desired flow rate (0- 80 kg m⁻² s⁻¹). After stationary regime is reached heating power (range 0 – 25 Wcm⁻²) is applied. All data are continuously monitored. When stationary regime is reached temperature and pressure profiles are recorded as well as flow rate, heating power...

4.2. Single-phase heat Transfer

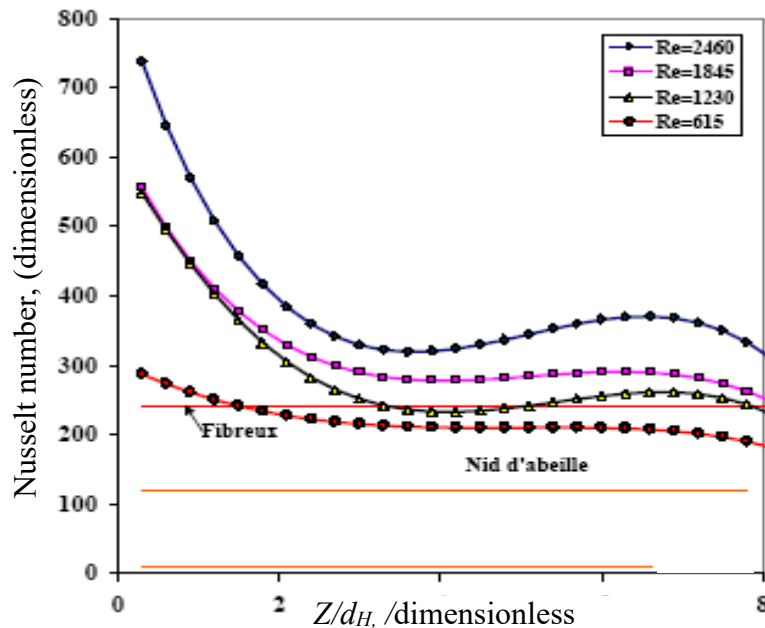


Figure 15: Experimental local Nusselt number profiles. Inserted foam and litterature data.

Figure 15 shows experimental local Nusselt number profile along main flow direction in the case of copper foam simply inserted in the channel (no welding with channel wall). The Nusselt number is based on channel hydraulic diameter and fluid thermal conductivity. One could remark the sharp decrease of Nusselt along the main flow axis that indicates macroscopic establishment of heat transfer and fluid flow. The entrance zone length is proportional to Reynolds number as expected as A

boundary layer model lead to a Nusselt number varying like $x^{-1/2}$. Outside the entrance zone variation of Nusselt number are mainly linked to experimental uncertainties on temperatures (about 0.1 °C and these transfer coefficients are deduced from local temperature difference.) and used interpolation technique [41].

High heat transfer coefficient is obtained compared to tube (increase of 2 orders of magnitude). These 3D foam present clearly better thermal performance than honeycomb structure, comparable to those obtained with sintered bronze fibers in similar conditions [3], but these performance are obtained for a pressure drop far smaller than the one of the fibers bed. Moreover, the fibers bed porosity is about 60 % thus at same metal mass thermo-hydraulic performance of the foam are far netter than those of the other structures. Influence of wall–foam contact is determinant on heat transfer phenomena as wall-foam heat transfer resistance is a limiting factor in thermal performance of such porous media [41].

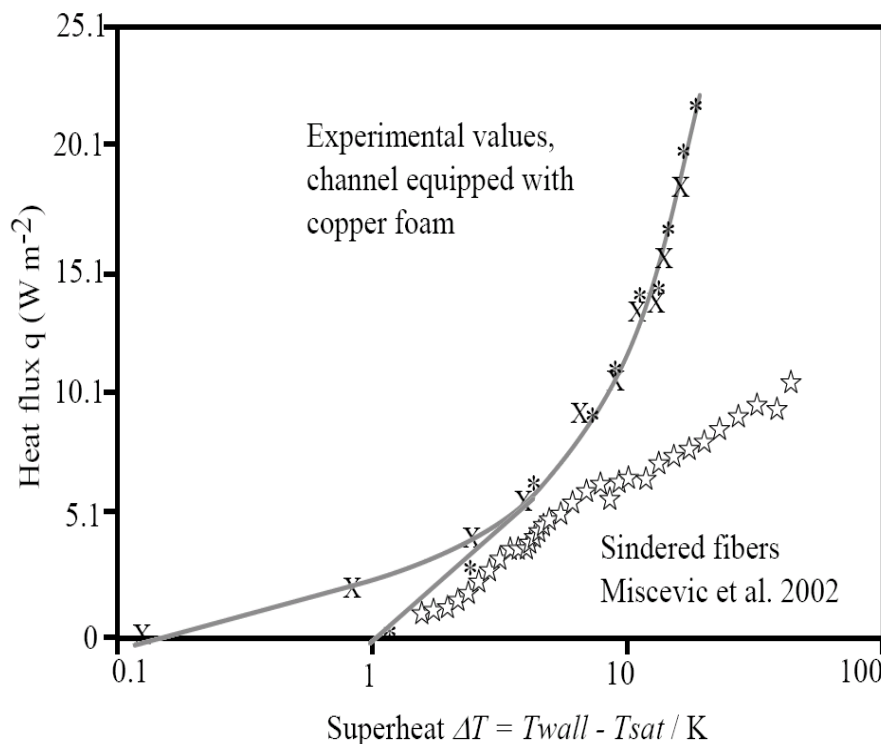


Figure 16: Boiling Curve: copper foam compared to sintered bronze fibers.
*: inserted; x: welded; stars: bronze fibers [42]

The boiling curve (Figure 16) shows the heat flux as a function of the wall superheat (ΔT : temperature difference between the wall and the fluid) in log-log scale. This curve was measured for two cases (i)

the foam welded to the wall and (ii) the foam just inserted in the channel. The onset of boiling starts at very low superheat ($\Delta T \sim 0.1$ and 1°C , respectively) compared to the “empty” channel whose ΔT is about 10°C . The heat flux strongly increases when the superheat increases. The fluid velocity has no influence on the heat flux, even at low superheat and very low fluid velocity ($10\text{--}40 \text{ kg m}^{-2}\cdot\text{s}^{-1}$). The critical heat flux, for which the walls dry out (formation of an insulating vapor film on the walls leading to a overheating), was not reachable with our set-up, and so, largely exceeds $30 \text{ kW}\cdot\text{m}^2$ even at lowest tested velocity.

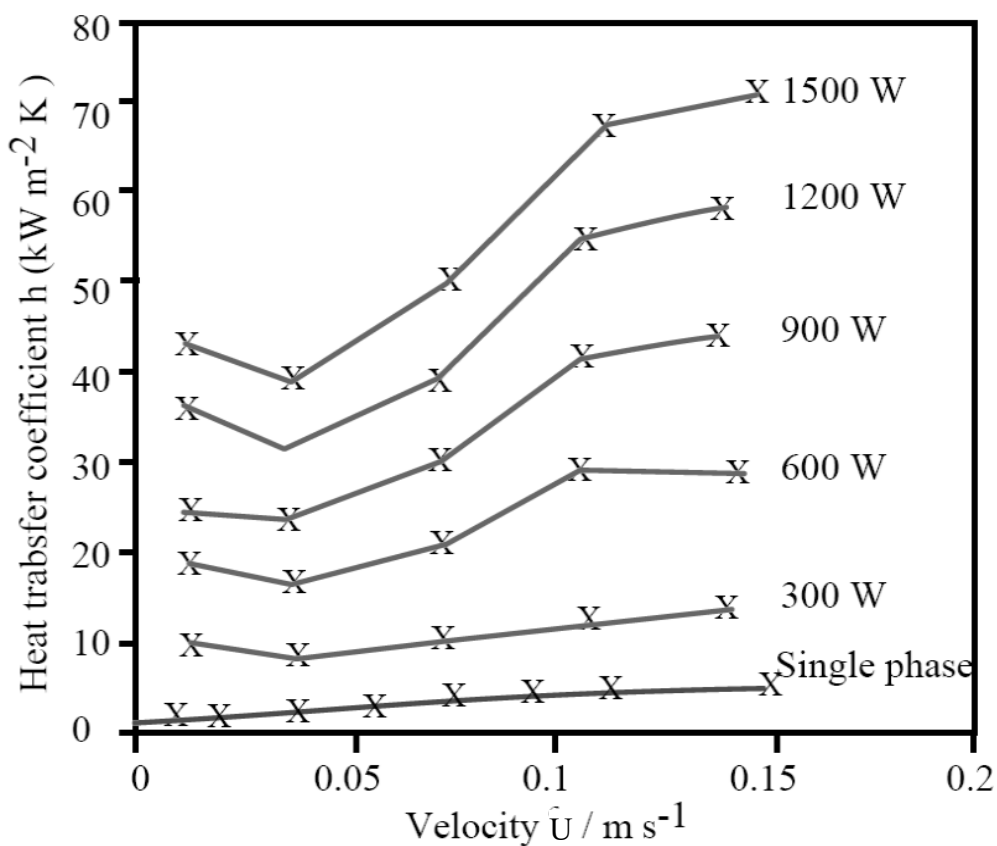


Figure 17: Boiling heat transfer coefficient in a rectangular channel equipped with welded copper foam versus liquid n-pentane velocity.

Performances of copper foam were compared to other fibrous materials. The boiling curve obtained in the same conditions for bronze sintered fibers, which are known for their high thermal performances [3] is similar to the foam inserted at low superheat. However, when the superheat exceeds 10°C , the heat flux is far smaller than the one obtained in the foam.

The high performance of the foam is linked to its open structure that permits an easy evacuation of the

vapor formed near the wall. This improves the heat transfer and avoids the phenomenon of dry out. Moreover, the pressure drop generated in the foam is 10 times smaller than those in the sintered fibers for the same heat transfer and velocity conditions.

We present, on figure 17, channel global heat exchange coefficient in boiling condition. We plotted the single-phase value and the variation of this coefficient in function of inlet liquid velocity for several heating power. This figure illustrates the very strong increase of heat transfer induced by liquid-vapor phase change phenomena.

For a given velocity the heat transfer coefficient is proportional to the heat flux in the studied boiling regime. This indicates a stable behavior (no risk of burn-out) of any biphasic heat exchanger working in these conditions of heat and mass flux.

5. Concluding Remarks

This work presents an original experimental method to determine the hydrodynamic characteristics of metallic foams. For this, the determination of the pressure profile along the channel is obtained using multiple pressure sensors. We determine single-phase flow laws for foam covering a wide range of pore size. Compressibility effects are studied and an adapted treatment of experimental data is proposed.

An expression modeling the dependence of inertial coefficient and permeability in function of morphology of the foam is proposed.

The adiabatic (air-water) conditions were analyzed. Results, reported in term of biphasic multipliers according to a simple homogeneous model, show up the impact of foam texture and gas quality on flow laws.

We developed an experimental methodology to analyze biphasic flow and heat transfer phenomena in metallic foam. This study illustrates the improvement of both single-phase and biphasic heat transfer given by the use of foam in a channel. The superheat at the onset of boiling is reduced and the heat transfer is increased. The flow laws in these materials are dominated by inertial effects, but the pressure drop generated in these materials remains very low. These results show a very strong impact of the foam structure on heat transfer and fluid flow.

6. Acknowledgments

The authors wish to thank Recemat Company and SCPS Company for providing the samples, and the French government financial support in the frameworks of a PACo programme and CNRS Energy program: PR Specimousse.

7. References

1. Ashby, M.F., et al., *Metal foams: A design guide* 2000, Boston, MA: Butterworth – Heinemann.
2. Banhart, J., *Manufacture, Characterization and application of cellular metals and metal foams*. Progress in materials Science, 2001. **46**: p. 529-532.
3. Tadriss, L., M. Miscevic, O. Rahli, and F. Topin, *About the Use of Fibrous Materials in Compact Heat Exchangers*. Experimental Thermal and Fluid Science, 2004. **28**: p. 193 – 199.
4. Sullines, D. and K. Daryabeige. *Effective thermal conductivity of high porosity open cell nickel foam*. in *35th AIAA Thermophysics Conference*. 2001. Anaheim, CA.
5. Vafai, K. and C.L. Tien, *Boundary and inertia effects on convective mass transfer in porous media*. int. J. Heat Mass Transfer, 1982. **25** (8): p. 1183-1190.
6. Catillon, S., et al. *Influence of Cellular Structure in catalytic reactors for H₂ Production: Application to Improvement of Methanol Steam Reformer by the Addition of a Copper Foam*. in *2nd France-Deutchland Fuel Cells Conference*. 2004. Belfort, France.
7. Du Plessis, J.P. and J.H. Masliyah, *Mathematical modeling of flow through consolidated isotropic porous media*. Transport in Porous Media, 1988. **3**: p. 145-161.
8. Du Plessis, P., M. A.;, J. Comiti , and J. Legrand, *Pressure Drop Prediction for Flow through High Porosity Metallic Foams*. Chem. Eng. Sci., 1994. **49**: p. 3545-3553.
9. Lu, T.J., H.A. Stone, and M.F. Ashby, *Heat transfer in open- cell metal foams*. Acta Materialia, 1998. **46**: p. 3619-3635.
10. Calmidi, V.V., *Transport phenomena in high porosity metal foam*. 1998, University of Colorado: Boulder, CO.
11. Calmidi, V.V. and R.L. Mahajan, *Forced convection in high porosity metal foams*. Journal of Heat Transfer, 2000. **122**: p. 557-565.
12. Fourie, J.G. and J.P. Du Plessis, *Pressure drop modelling in cellular metallic foams*. Chemical Engineering Science, 2002. **57**(14): p. 2781-2789.
13. Boomsma, K. and D. Poulikakos, *The effects of compression and pore size variations on the liquid flow characteristic in metal foams*. Journal of fluids engineering, 2002. **124**: p. 263-272.
14. Boomsma, K. and D. Poulikakos, *On the effective thermal conductivity of a three-dimensionally structured fluid-saturated metal foam*. International Journal of Heat and Mass Transfer 2001. **44**: p. 827-836.
15. Bhattacharya, V., R. Calmidi, and L. Mahajan, *Thermophysical properties of high porosity metal foams*. Int. J. Heat Mass Transfer, 2002. **45**: p. 1017-1031.
16. Bastawros, A.F. *Effectiveness of open-cell metallic foams for high power electronic cooling*. in *Symposium on the Thermal Management of Electronics (IMECE)*. 1998. Anaheim, CA.
17. Decker, S., S. Möbbauer, D.T. Nemoda, and T. Zapf. *Detailed Experimental Characterization and Numerical Modeling of Heat and Mass Transport Properties of Highly Porous Media for Solar Receivers and Porous Burners*. in *Lehrstuhl für Strömungsmechanik Universität Erlangen-Nürnberg Cauerstr.* 2000. Erlangen, Germany.
18. Writz, R.A. *A semi-empirical model for porous media heat exchanger design*. in *the American Society of Mechanical Engineers National Heat Transfer Conference*. 1997. Baltimore, MD.
19. Kim, S.Y., B.H. Kang, and J.-H. Kim, *Forced convection from aluminum foam materials in an asymmetrically heated channel*. International Journal of Heat and Mass Transfer, 2001. **44**(7): p. 1451-1454.
20. Madani, B., F. Topin, L. Tadriss, and F. Rigollet, *Flow laws in metallic foams: experimental determination of inertial and viscous contribution*. Journal of porous media, 2006. **In press**.
21. Langlois, S. and F. Coeuret, *Flow-through and flow-by porous electrodes of nickel foam. I. Material characterisation*. journal of applied electrochemistry, 1989. **19**: p. 43-50.
22. Phanikumar, M.S. and R.L. Mahajan, *Non-Darcy natural convection in high porosity metal foams*. International Journal of Heat and Mass Transfer, 2002. **45**: p. 3781–3793.
23. Zhao, C.Y., T. Kim , T.J. Lu, and H.P. Hodson, *Thermal Transport Phenomena in Porvair. Metal Foams and Sintered Beds*, in *Technical report*. 2001, Micromechanics Centre & Whittle Lab Department of Engineering - University of Cambridge.
24. Topin, F., J.P. Bonnet, and L. Tadriss. *Multiphase flow in metallic foam: Experimental analysis of flow laws*. in *4th Int. Conf. on "Porous Metals and Metal Foaming Technology*. 2005. Kyoto, Japan.
25. Vicente, J., J.V. Daurelle, F. Topin, and L. Tadriss. *Structural properties measurement: A Morphological tool for transport properties determination* in *4th Int. Conf. on "Porous Metals and Metal Foaming Technology*. 2005. Kyoto, Japan.

26. Vicente, J., F. Topin, and J.V. Daurelle, *Open celled material structural properties measurement: from morphology to transport properties*. Material transaction, 2006. **In press**.
27. Renard, P., A. Genty, and F. Stauffer, *Laboratory détermination of the full permeability tensor*. Journal of geophysical research, 2001. **106(B11)**: p. 26443-26452.
28. Darcy, H.P.G., *Exposition et application des principes à suivre et des formules à employer dans les questions de distribution d'eau. Les fontaines publiques de la ville de Dijon*. 1856, Paris: Victor Delmont.
29. Fourar, M., G. Radilla, R. Lenormand, and C. Moyne, *On the non-linear behavior of a laminar single-phase flow through two and three-dimensional porous media*. Advances in Water Resources 2004. **27**: p. 669-677.
30. Bonnet, J.P., F. Topin, and L. Tadrist. *Etude expérimentale de l'impact de la compressibilité et du changement de phase sur les lois d'écoulement en milieux poreux cellulaire ouverts*. in *SFT'05*. 2005. Reims, France.
31. Wallis, G., *One-Dimensional Two-Phase Flow* 1969, New-York, NY: Mc graw Hill.
32. Hunt, M.L. and C.L. Tien, *Effects of thermal dispersion on forced convection in fibrous media*. Int. J. Heat Mass Transfer, 1988. **31**: p. 301-309.
33. Khayargoli, P., V. Loya, L.P. Lefebvre, and M. Medraj. *The impact of microstructure on the permeability of metal foams*. in *CSME 2004 Forum*. 2004. London, Ontario.
34. Paek, J.W., B.H. Kang, S.Y. Kim, and J.M. Hyun, *Effective thermal conductivity and permeability of aluminum foam materials*. International Journal of Thermophysics, 2000. **21(2)**: p. 453-464.
35. Moreira, E.A., M.D.M. Innocentini, and J.R. Cour, *Permeability of ceramic foams to compressible and incompressible flow*. Journal of the European Ceramic Society 2004. **24**: p. 3209-3218.
36. Innocentini, M.D.M., R.V. Salvini, A. Macedob, and V.C. Pandolfelli, *Prediction of Ceramic Foams Permeability Using Ergun's Equation*. Materials Research , , 1999. **Vol. 2(No. 4)**: p. 283-289.
37. Grall, V., *Etude expérimentale d'écoulements diphasiques liquide-gaz en mini canaux et en milieu poreux modèle*. 2001, Institut National Polytechnique de Toulouse: Toulouse.
38. Kaviany, M., *Principles of heat transfer in porous media*. Mecanical Engineering Series. 1992: Springer-Verlag.
39. Jamialahmadi, M., H. Muller-Steinhagen , and M.R. Izadpanah, *Pressure drop, gas hold-up and heat transfer during single and two-phase flow through porous media*. International Journal of Heat and Fluid Flow 2005. **26**: p. 156-172.
40. Madani, B., F. Topin, and L. Tadrist. *Ebullition convective dans les mousses métalliques : Analyse expérimentale des effets de contact matrice solide -paroi*. in *Congrès de la SFT 04*. 2004. Giens, France.
41. Madani, B., F. Topin, L. Tadrist, and K. Bouhadeh. *Mesure du coefficient de transfert de chaleur local paroi-fluide dans un canal à mousse métallique en écoulement liquide et en ébullition*. in *12ième JITH*. 2005. Tanger, Maroc.
42. Miscovic, M., F. Topin, and L. Tadrist, *Convective boiling phenomena in a sintered fibrous channel: Study of thermal non-equilibrium behavior* Journal of Porous Media, 2002. **5(4)**: p. 229-239.